NeuroImage: Clinical 6 (2014) 32–42

Contents lists available at ScienceDirect

NeuroImage: Clinical

journal homepage: www.elsevier.com/locate/ynicl

Cellular correlates of longitudinal diffusion tensor imaging of axonal degeneration following hypoxic–ischemic cerebral infarction in neonatal rats

Ursula I. Tuor[a,b,c,d,*], Melissa Morgunov[b,c], Manasi Sule[b,c], Min Qiao[b,c], Darren Clark[a,d,e], David Rushforth[b], Tadeusz Foniok[b], Adam Kirton[a,d,f]

[a] Hotchkiss Brain Institute, Faculty of Medicine, University of Calgary, Calgary, T2N 4N1, Canada
[b] Experimental Imaging Centre, Faculty of Medicine, University of Calgary, Calgary, AB T2N 4N1, Canada
[c] Departments of Physiology and Pharmacology, Faculty of Medicine, University of Calgary, Calgary, AB T2N 4N1, Canada
[d] Department of Clinical Neurosciences, Faculty of Medicine, University of Calgary, Calgary, AB T2N 4N1, Canada
[e] Department of Medical Physics and Informatics, School of Medicine, University of Szeged, Szeged, Hungary
[f] Department of Pediatrics, Alberta Children's Hospital Research Institute, Faculty of Medicine, University of Calgary, Calgary, AB T2N 4N1, Canada

ARTICLE INFO

Article history:
Received 1 May 2014
Received in revised form 14 July 2014
Accepted 4 August 2014
Available online 7 August 2014

Keywords:
Magnetic resonance imaging
Cerebral peduncle
Neonatal cerebral hypoxia–ischemia
Myelination
Neurofilament
Glial activation

ABSTRACT

Ischemically damaged brain can be accompanied by secondary degeneration of associated axonal connections e.g. Wallerian degeneration. Diffusion tensor imaging (DTI) is widely used to investigate axonal injury but the cellular correlates of many of the degenerative changes remain speculative. We investigated the relationship of DTI of directly damaged cerebral cortex and secondary axonal degeneration in the cerebral peduncle with cellular alterations in pan-axonal neurofilament staining, myelination, reactive astrocytes, activation of microglia/macrophages and neuronal cell death. DTI measures (axial, radial and mean diffusivity, and fractional anisotropy (FA)) were acquired at hyperacute (3 h), acute (1 and 2 d) and chronic (1 and 4 week) times after transient cerebral hypoxia with unilateral ischemia in neonatal rats. The tissue pathology underlying ischemic and degenerative responses had a complex relationship with DTI parameters. DTI changes at hyperacute and subacute times were smaller in magnitude and tended to be transient and/or delayed in cerebral peduncle compared to cerebral cortex. In cerebral peduncle by 1 d post-insult, there were reductions in neurofilament staining corresponding with decreases in parallel diffusivity which were more sensitive than mean diffusivity in detecting axonal changes. Ipsilesional reductions in FA within cerebral peduncle were robust in detecting both early and chronic degenerative responses. At one or four weeks post-insult, radial diffusivity was increased ipsilaterally in the cerebral peduncle corresponding to pathological evidence of a lack of ontogenic myelination in this region. The detailed differences in progression and magnitude of DTI and histological changes reported provide a reference for identifying the potential contribution of various cellular responses to FA, and, parallel, radial, and mean diffusivity.

1. Introduction

Inadequate blood flow to the brain, termed cerebral ischemia, will produce brain injury and a progression of pathophysiological responses associated with energy depletion that include cell swelling, cytotoxic edema, vasogenic edema and if sufficiently severe or prolonged, neuronal cell death. When brain regions are directly damaged by ischemia this can lead to secondary injury or degeneration in associated axonal connections such as the corticospinal tracts. Detection of such changes on early subacute diffusion MRI have been described as "early" or "pre" Wallerian degeneration following perinatal stroke in neonates (De Vries et al., 2005; Kirton et al., 2007). Such early signs of Wallerian degenerative injury are predictive of specific functional outcomes and may improve prognostication, guide rehabilitation, and could represent both a selection criteria and potential novel target for clinical trials. In particular, if there is diagnostic evidence for early degenerative injury, such as increases in the intensity of the corticospinal tract in diffusion weighted magnetic resonance (MR) images, then prognosis for a good recovery in such infants has consistently been poor (Domi et al., 2009; Kirton et al., 2007; van der Aa et al., 2011). Understanding better the cellular responses that evolve with axonal degeneration following

Abbreviations: MR, magnetic resonance; DTI, diffusion tensor imaging; ADC, apparent diffusion coefficient of water; FA, fractional anisotropy; GFAP, glial fibrillary acidic protein; MBP, myelin basic protein.

* Corresponding author at: Depts of Physiology and Pharmacology, Clinical Neurosciences, and, Radiology, Univ. of Calgary, Teaching, Research and Wellness Building, Room P2E36, 3280 Hospital Drive N.W., Calgary, AB T2N 2T8, Canada.

http://dx.doi.org/10.1016/j.nicl.2014.08.003

stroke are important considering both their potential contributions to diagnosis and the potential for providing novel targets for therapeutic intervention. Currently, the tissue alterations underlying these MR biomarkers are unknown and speculative because histopathology, if available, is usually performed at single and relatively chronic time points many weeks to months after an ischemic insult.

Studies of the evolution of ischemic brain damage or infarction at subacute and chronic times has been assessed using standard MR imaging sequences such as T_2 or diffusion weighted imaging (Latchaw et al., 2009). Detecting secondary axonal or Wallerian degeneration is also possible with standard MR sequences. We recently demonstrated that following neonatal hypoxia with unilateral transient ischemia there is evidence for early Wallerian degeneration visible as either decreases in the apparent diffusion coefficient (ADC) and magnetization transfer ratio or increases in DW or T2 (Lama et al., 2011; Tuor et al., 2013) which pseudonormalize transiently. In these studies, the early corticospinal axonal changes (e.g. in the cerebral peduncle) reflected several cellular alterations such as a reduced staining for phosphorylated neurofilament H and increased vacuolation in hematoxylin and eosin stained sections.

DTI holds additional promise for detecting specific degenerative responses because of its potential sensitivity to certain ultrastructural cellular changes depending on the measured DTI parameter — i.e. fractional anisotropy, mean diffusivity and parallel or radial diffusivity. Of the extensive cellular responses produced by ischemia, those considered most likely to affect the diffusion properties of water are those that involve morphological tissue changes such as necrosis, astrogliosis, loss of myelin, loss of axonal neurofilaments or cellular inflammation (i.e. microglial/macrophage activation) (Nucifora et al., 2007; Zhang et al., 2012). Our group and others have shown that corticospinal tract DTI alterations are strongly correlated with motor outcome in children with perinatal stroke (Hodge, 2013; Roze et al., 2012; van der Aa et al., 2011). However the progression of DTI changes and whether there are differences between the evolution of cellular responses in direct ischemically injured brain versus associated connected tracts is not known. Differences are expected considering the different cellular compositions, for example neuronal rich cerebral cortex compared to axonal bundles within the descending corticospinal tract. A differential timing of DTI alterations is also expected considering direct ischemic injury is thought to be followed by a delayed Wallerian degeneration (Lama et al., 2011; Tuor et al., 2013). In order to better understand the unique cellular and DTI imaging alterations associated with secondary Wallerian degeneration relative to the onset and progression of direct ischemically damaged brain, it is necessary to compare their progression directly at multiple time points.

In the current study we hypothesized that DTI imaging would provide measures of progressive tissue changes within axonal tracts distal to the ischemic injury distinct from those in directly injured brain (e.g. cerebral cortex) and these differences would correspond with specific tissue morphological alterations in response to ischemia. This was investigated by using a neonatal rat model of unilateral transient cerebral hypoxia–ischemia and measuring DTI changes in the parietal cerebral cortex compared with its associated descending corticospinal tract axon fibers within the cerebral peduncle. DTI measurements were made at acute, subacute and chronic times after hypoxia–ischemia along with processing of brains at each of these time points to assess immunohistochemically potential contributions of morphological modifications. We focused on using markers for detecting cell death in neurons, loss of myelin and loss of neurofilaments in axons, and, activation of astrocytes and microglia/macrophages.

2. Material and methods

2.1. Model of hypoxia–ischemia

Fifty one pups delivered from 9 different pregnant Wistar female rats (Charles River Laboratories, Montreal, Canada) were used in the study. Experiments followed the Canadian Council on Animal Care guidelines and were approved by a University of Calgary Animal Care Committee. A moderate unilateral ischemic lesion with hypoxia (Vannucci and Vannucci, 2005) was produced as described previously (Lama et al., 2011; Qiao et al., 2009; Tuor et al., 2013). Briefly, pups ($n = 38$) on their 7th day of life had their right common carotid artery ligated under isoflurane anesthesia followed by a 60 minute exposure to hypoxia in a chamber containing 8% O_2 and 92% N_2 at 35.5 °C. Sham control animals ($n = 13$) experienced a similar surgical procedure without carotid artery ligation and hypoxia exposure. The Vannucci model of neonatal cerebral hypoxia–ischemia (Vannucci and Vannucci, 2005) produces ischemic damage and infarction within the distribution of the middle cerebral artery territory. Thus, the parietal *cortex* was selected as a representative brain region of *direct* hypoxic–ischemic damage or infarction. The posterior *cerebral peduncle* supplied by the posterior circulation was selected as a region of *secondary injury* remote to the hypoxia–ischemia but with axonal connections to directly damaged regions. Brain near the aqueduct in the posterior *pons* was selected as a control region generally unaffected by the hypoxia–ischemia.

2.2. Acquisition of MR images

Sham animals or animals subjected to cerebral hypoxia–ischemia were anesthetized (1.5–2% isoflurane) and DTI images in addition to anatomical scans were acquired at 3 h, 1 d, 2 d, 1 w or 4 w post-insult. Anatomical images were also acquired at 1 d post insult in the chronic animals (1 or 4 w) to confirm the extent of ischemic damage. MR images were acquired using a 9.4 T Bruker Biospin MR imaging system and Paravision 5.1 software. Throughout the scanning, respiration was monitored and maintained by adjustments in anesthesia and body temperature was maintained using a feedback heated air system (Small Instruments Inc., Stony Brook, NY). Images were acquired using a 3.5 cm diameter quadrature volume coil for radiofrequency transmission and reception. The head and body was restrained using custom designed swaddling and a head band or ear pins. Depending on the age of the animal, each MR imaging scan consisted of 25–30 slices of 0.5–0.55 mm thick covering the cerebrum and medulla, a 2×2 cm^2 or 2.5×2.5 cm^2 field of view and a data matrix size of 128×128. Anatomical T_2 maps were first generated using a T_2 imaging sequence consisting of a set of T_2 weighted spin echo images with 32 echoes, repetition time of 10 s and echo time of 10 ms between echoes. For DTI, a four-shot echo-planar imaging sequence was used to acquire four averages of sets of diffusion weighted images. These were acquired with b values of 0 (5 images) and 1000 s/mm^2 (30 images in non-collinear directions) using a repetition time of 6500 ms and an echo time of 35 ms. Artifacts associated with imperfections in the radio frequency pulse, gradient stability, and gradient echo currents were removed using a navigator-echo phase correction. Nyquist ghost artifacts were suppressed in the image reconstruction using information acquired during the initial automatic receiver gain adjustment. DTI Image acquisition time was approximately 1 h.

2.3. Analysis of MR images

T2 weighted images were visualized using local MR analysis software (Marevisi, National Research Council of Canada, Winnipeg, Canada). These images were used to assess the extent of ischemic damage and measure brain volumes (atrophy). Inspection of T2 images was also used to exclude from further analysis animals with no cortical T2 lesions or very large hyperintense lesions extending into the pons. They were also used to identify anatomical landmarks for selection of the regions of interest in subsequent DTI analysis and histological analysis as identified using a rat brain atlas (Paxinos and Watson, 1998). These regions of interest were manually defined in the MR images and histological sections and included the cerebral peduncle (0.3–0.4 mm^2), pons (within the central gray and mesencephalic trigeminal nucleus regions, 0.6–0.9 mm^2) and parietal cortex (0.7–1.0 mm^2) for areas both ipsilateral and contralateral to the lesion containing hemisphere. Once the ischemic infarct had

progressed towards cavitation and cyst formation (i.e. 1 and 4 w post-hypoxia–ischemia), homologous measures of cortical tissue were not possible and therefore were taken adjacent to the cyst — a peri-cyst cortical region (0.4–0.6 mm^2). Sizes and shapes were adjusted using the contralateral region (e.g. cerebral peduncle) as a guide and areas of interest were adjusted if there was atrophy in order to minimize partial volume effects.

Diffusion tensor images were imported into DTI Studio (Jiang et al., 2006) through the DTI mapping function as Philips REC files. Image parameters, the gradient table and image files were also imported. Coregistration errors and motion compromised images were removed prior to analysis. Entire scans were excluded if less than eighteen artifact free images were available per slice. The minimum of eighteen directions was selected empirically as the cut-off following an analysis of 12 test data sets with repeatedly fewer b directions (e.g. 25, 22, 20, 18, 16 and 15 compared to 30) which demonstrated no significant effect of a reduction in the number of b directions except for FA and L3; and, those were altered only once the number of directions was 16 or less ($p < 0.05$, repeated ANOVA). For each image slice the DTI program calculated the over-determined matrix, the ADC vector and the pseudo-inverse of the matrix using singular value decomposition in order to compute the tensor for each pixel (Jiang et al., 2006). Imaging maps were then calculated for the mean diffusivity (ADC; $(\lambda1 + \lambda2 + \lambda3) / 3$), the parallel diffusivity ($\lambda1$), the radial diffusivity ($(\lambda2 + \lambda3) / 2$) and the fractional anisotropy (FA). Measures of the DTI variables were obtained within regions of interest manually drawn ipsilateral and contralateral (non-ischemic damaged side) of the brain slice. Differences in ipsilateral and contralateral values were converted to a percentage of contralateral.

2.4. Histological processing of brains

Following their last MR scan, subgroups of animals were perfused transcardially with 10% formalin under deep pentobarbital anesthesia and their brains were embedded in paraffin. Brains from 44 rats were processed and stained for 5 different cellular or injury markers within sections containing the parietal cortex, posterior cerebral peduncle and central gray region of the pons. Thirteen of these animals were sham controls and 31 were animals subjected to hypoxia–ischemia and euthanized at the 5 different times post hypoxia–ischemia (n = 4–7/group). Sections (6 μm thick) were cut at the level of the posterior cerebral peduncle and parietal cortex using the brain atlas and anatomical landmarks to match sections to the MR slices and measure staining changes in equivalent regions of interest to those for the MR images.

Sections from each region were stained for a marker of cell death or degenerating neurons using fluorojade B (Schmued and Hopkins, 2000) according to the manufacturer's instructions (Millipore, Billerica, MA, USA). Briefly, deparaffinized sections were exposed to 0.06% potassium permanganate for 15 min washed in distilled water and then stained with 0.0004% fluorojade solution.

Sections at each level were also processed immunohistochemically to stain for the following: neurofilaments using a pan-axonal neurofilament marker (monoclonal SMI312), reactive astrocytes using anti-glial fibrillary acidic protein (GFAP), activated microglia/macrophages using anti-CD68/ED1, and, myelin using an antibody against myelin basic protein (MBP). Sections were deparaffinized and processed for antigen retrieval by boiling in sodium citrate (pH = 6.0, 90 °C) for 10 min then washed in PBS. Slides were subsequently blocked with 1% H_2O_2 in methanol for 5 min followed by 10% goat serum in 0.1 M PBS and then a PBS wash. Slides were then incubated for 1 h at room temperature with one of 4 different primary antibodies: SMI312 antibody (1:1000 in BSA, Covance, Berkeley, CA, USA), polyclonal rabbit anti-GFAP (1:500 in BSA, Diagnostics Canada Inc., ON, Canada), mouse anti-rat CD68/ED1 (1:500 in BSA, AbD Serotec, Raleigh, NC, USA) or rabbit anti-MBP (1:500 in BSA, Chemicon International, CA, USA). Following a PBS wash, slides were incubated overnight at 4 °C with the appropriate secondary antibody, either biotinylated goat anti-rabbit IgG or biotinylated goat anti-mouse IgG (1:400 in BSA, Jackson ImmunoResearch Lab Inc., PA, USA). This was followed by incubation for half an hour with horseradish peroxidase-streptavidin (1:400 in PBS, Diagnostics Canada Inc., ON, Canada). Finally, positive cells were visualized following an application of 3,3-diaminobenzidine (Sigma Aldrich, MO, USA) dissolved in 0.3% H_2O_2 in distilled water for approximately 3 min.

2.5. Analysis of histological sections

The histological sections were assessed semi-quantitatively for changes in staining within the regions of interest either by measuring optical density or by quantifying numbers of positively stained cells per field of view. For optical density measures, sections stained with either SMI312, GFAP or MBP were first captured digitally using a scanner (Nikon Scan, version 4, Nikon Inc.). These images were converted to gray images and mean gray levels (ImageJ, NIH) were measured within the same regions of interest as those drawn for the MR brain slices. Regions with less intense staining had higher mean gray values. The ipsilateral versus contralateral differences in gray levels were converted to a percentage of the contralateral value.

The CD68/ED1 and fluorojade stained sections were analyzed using digitized microscopy (Microbrightfield, Olympus, 40× magnification). The numbers of positively stained cells per field of view were estimated within regions corresponding to those selected from MR images. Three different fields of view were counted for positive staining cells by an investigator (M.S.) blinded to treatment. The mean of these provided an average for each animal for each region.

2.6. Statistical analysis

All group data is reported as mean ± SD and statistical comparisons were considered significant at $P < 0.05$. Measured values within different brain regions were considered to be repeated measures within an animal. A two way repeated analysis was used to determine significant region and time interactions and these were followed by a Holm–Sidak test for multiple comparisons. Statistical tests were performed using SigmaPlot (Systat Software Inc, San Jose, CA). To convey clearly the differences for the cerebral peduncle, we noted in the graphs only the significant differences for this region. The correlation between histological changes and DTI parameters was assessed using a Pearson Product correlation analysis within each time point or all time points with a Bonferroni adjustment for multiple comparisons.

3. Results

3.1. MR imaging

3.1.1. T2 imaging of anatomy and atrophy

Acutely following cerebral hypoxia–ischemia, T_2 MR images presented with areas of hyperintensity within the territory typically supplied by the middle cerebral artery, as described previously (Lama et al., 2011; Tuor et al., 2013). Very bright cystic areas developed in regions of infarction such as the parietal cortex by 1 or 4 w post-insult. In regions remote from infarction, loss of brain volume provided evidence for atrophy at 1 and 4 wk post-insult. We measured brain volume in the ventral pons at the level of the posterior cerebral peduncle to be similar in left and right hemispheres at hyperacute and acute times but significantly ($P < 0.01$) decreased ipsilateral to the ischemic damage, at 1 and 4 w post insult (i.e. left–right differences in volume of $-2 \pm 9\%$, $-1 \pm 8\%$, $9 \pm 9\%$, $21 \pm 8\%$ and $27 \pm 5\%$ at 3 h, 1 d, 2 d, 1 w and 4 w post-insult, respectively).

3.1.2. DTI imaging

Forty-five DTI images were acquired. Eight were excluded due to excessive motion, one due to T_2 ischemic lesions extending contiguously

into the posterior pons and one due to a lack of any T_2 cerebral lesions (i.e. infarction). This resulted in successful DTI image analysis in sham controls and 5 groups of animals at various times post hypoxia–ischemia (3 h, 1 d, 2 d, 1 w and 4 w with $n = 8, 6, 7, 3$ and 4, respectively). The 3 h DTI imaging group was perfusion fixed approximately 4 h post hypoxia–ischemia. Mean contralateral diffusion tensor parameters were not different from mean sham values for the respective regions and time points.

3.1.3. ADC and parallel diffusivity imaging

In the cerebral cortex, inspection of ADC maps had evidence of reductions in ADC in the parietal cortex acutely (3 h–2 d) followed by cyst development or normalization in pericystic cortex thereafter (Fig. 1A–E). This was confirmed by quantitative analysis (Fig. 1F, cyst — dashed bar). Analogous to ADC, the parallel diffusivity (λ1) maps (Fig. 1L–P) had ischemic-related decreases in the parietal cortex; and, quantitatively these were similar to those of the ADC changes (Fig. 1Q).

In contrast, within the cerebral peduncle, a region with axonal connections to ischemically injured tissue, there were reductions in ADC and parallel diffusivity that were not apparent until 1 d following hypoxia–ischemia (e.g. Fig. 1H, I, S, T, U, V). Quantitative analysis demonstrated that these reductions were delayed until and maximal at 1 d (Fig. 1F, Q). Following 1 d, the decrease in ADC and parallel diffusivity ipsilaterally in the cerebral peduncle was significantly less pronounced (Fig. 1F, Q). Ipsilateral reductions in parallel diffusivity remained significant at the 1 and 4 w time points.

In the pons, intensities appeared homogenous and similar in both hemispheres (Fig. 1G–K, R–V). Quantitatively, ipsilateral and contralateral measures of ADC or parallel diffusivity were similar (Fig. 1F, Q) and differed from cerebral peduncle at a number of time points.

3.1.4. Radial diffusivity

In the parietal cortex at acute times (3 h to 2 d) following cerebral hypoxia–ischemia, the radial diffusivity was reduced ipsilaterally (e.g. Fig. 2A–C). This was reflected in the quantitative analysis with reductions being maximal at 3 h (Fig. 2F). In the cerebral peduncle, the radial diffusivity was also reduced ipsilaterally at acute times but this was not apparent until 1 d post insult (e.g. Fig. 2G–I). Furthermore, in the cerebral peduncle the reductions were maximal at 1 d post-insult progressing to a significant increase ipsilaterally at 1 w post insult. In the pons, in contrast to the cerebral peduncle, the radial diffusivity was generally similar in ipsilateral and contralateral hemispheres for all time points.

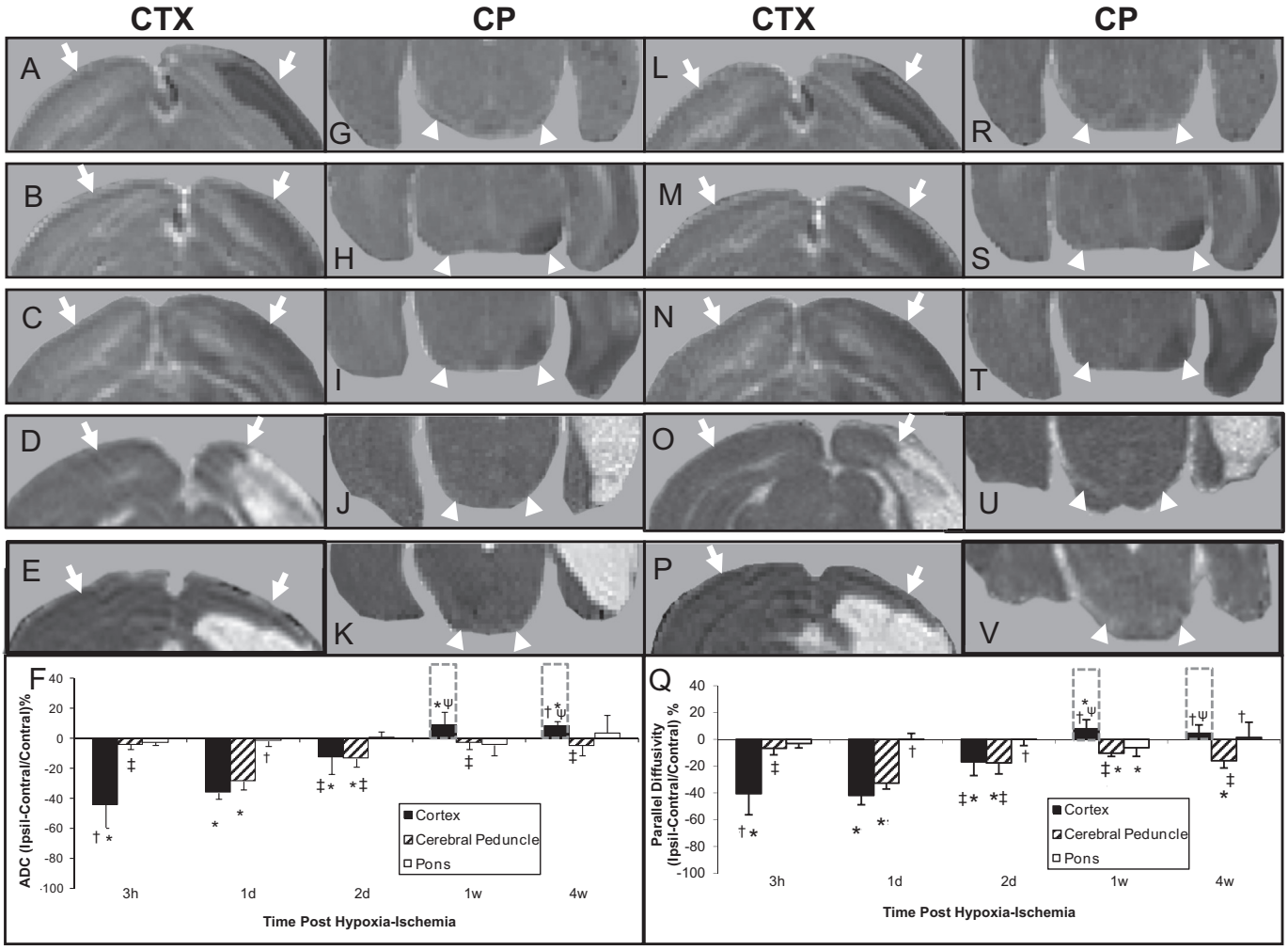

Fig. 1. Magnetic resonance imaging maps of the apparent diffusion coefficient of water (ADC) (A–K) and its parallel diffusivity (L–V) analyzed from diffusion tensor imaging scans of neonatal rat brains at 3 h (top row, A, G, L, R), 1 d (second row, B, H, M, S), 2 d (third row, C, I, N, T), 1 w (fourth row, D, J, O, U) or 4 w (fifth row, E, K, P, V) after transient hypoxia + right cerebral ischemia. Shown are representative maps of slices containing the cerebral cortex (A–E, L–P, arrows) and the posterior cerebral peduncle (G–K, R–V, arrow heads). Mean (±SD) values of ipsilateral–contralateral differences presented as a percentage of contralateral are shown in F and Q. Development of cyst is shown as off-scale measures in a dashed line bar above pericyst cortical measures. $^{*}P < 0.05$; ipsilateral different from contralateral; $^{\dagger}P < 0.05$, cortex or pons different from cerebral peduncle within the time point; $^{\ddagger}P < 0.05$, different from corresponding region at 1 d; $^{\Psi}P < 0.05$ different from corresponding region at 3 h, 1 d and 2 d (Two Way repeated ANOVA, Holm–Sidak multiple comparisons).

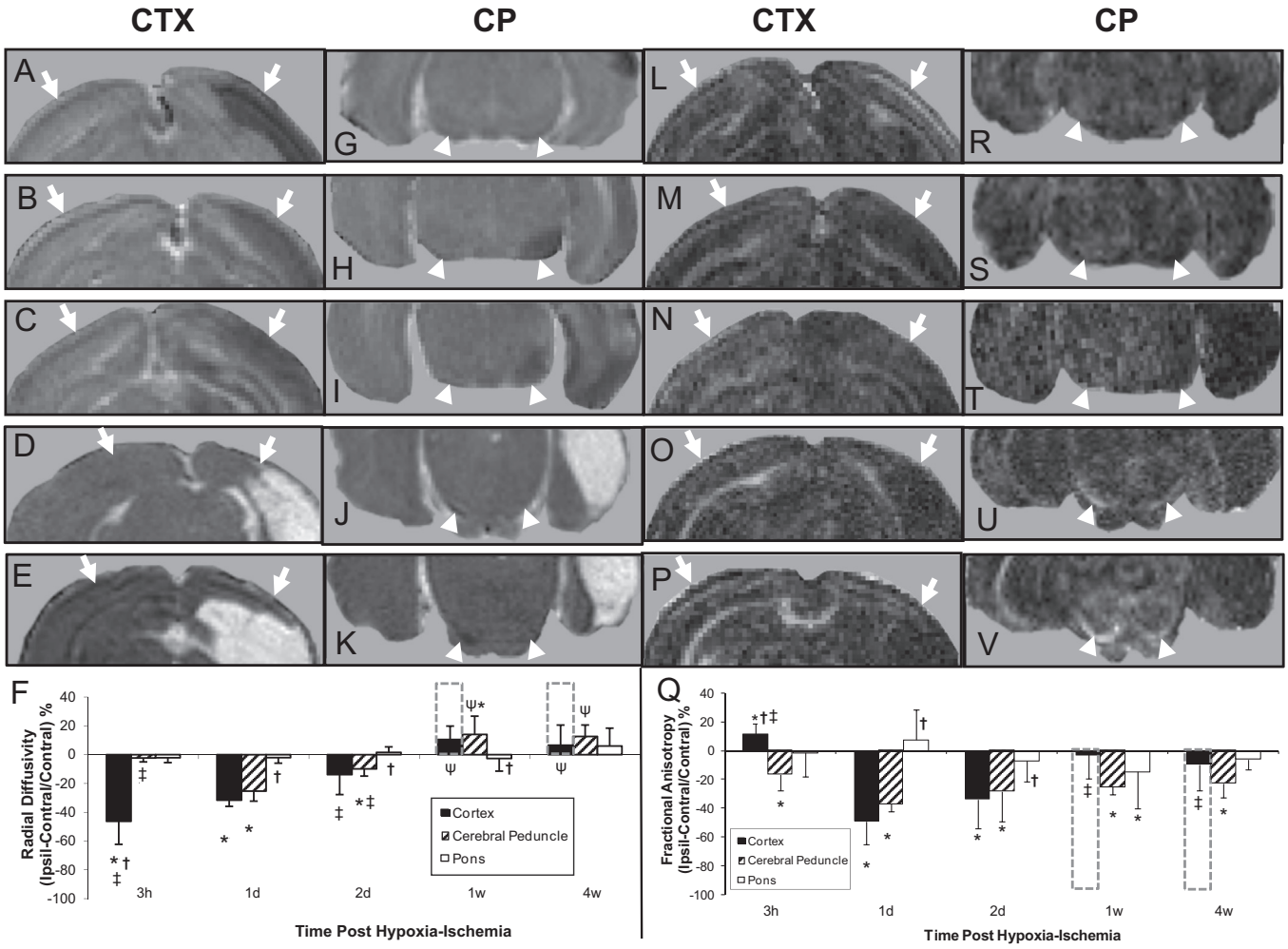

Fig. 2. Magnetic resonance imaging maps of the radial diffusivity (A–K) and the fractional isotropy (L–V) analyzed from diffusion tensor imaging scans of neonatal rat brains at 3 h (top row, A, G, L, R), 1 d (second row, B, H, M, S), 2 d (third row, C, I, N, T), 1 w (fourth row, D, J, O, U) or 4 w (fifth row, E, K, P, V) after transient hypoxia + right cerebral ischemia. Shown are representative maps of slices containing the cerebral cortex (A–E, L–P, arrows) and the posterior cerebral peduncle (G–K, R–V, arrow heads). Mean (±SD) values of ipsilateral–contralateral differences presented as a percentage of contralateral are shown in F and Q. Development of cyst is shown as off-scale measures in a dashed line bar above pericyst cortical measures. $^{*}P < 0.05$; ipsilateral different from contralateral; $^{\dagger}P < 0.05$, cortex or pons different from cerebral peduncle within the time point; $^{\ddagger}P < 0.05$, different from corresponding region at 1 d; $^{\Psi}P < 0.05$ different from corresponding region at 3 h, 1 d and 2 d (Two Way repeated ANOVA, Holm–Sidak multiple comparisons).

3.1.5. Fractional anisotropy

In the parietal cortex at the hyperacute time point (3 h) following hypoxia–ischemia, there was an increase in FA followed by ipsilateral decreases at 1 and 2 d and a normalization within peri-cyst regions at 1 and 4 w (Fig. 2L–P, Q). In contrast, in the cerebral peduncle, FA was reduced ipsilaterally at all time points (Fig. 2R–V) with the left–right differences being significant and no appreciable progression over time.

3.2. Histological changes

3.2.1. Reduction in pan-axonal neurofilament staining detection with SMI312

Brains of sham animals stained with SMI312 had no visible alterations in staining levels bilaterally (e.g. Fig. 3A) and there were no quantitative left–right differences in gray levels. In brains of animals exposed to HI, there were higher gray levels and visible decreases in staining of SMI312 within the parietal cortex (sections not shown) at acute time points (3 h and 1 d). This was reflected in quantitative differences which were less pronounced in peri-infarct cortex chronically (Fig. 3F). In the cerebral peduncle, brighter regions of reduced SMI312 staining ipsilaterally were also observed but not until 1 d post hypoxia–ischemia and thereafter (e.g. Fig. 3B–E). Quantitative analysis of gray levels in SMI312 stained sections demonstrated significant ipsilateral–contralateral increases in gray levels at acute and chronic times (Fig. 3F). In the pons, a region generally unaffected by HI, there were no significant left–right differences in SMI312 staining following HI.

3.2.2. Changes in myelination detected with myelin basic protein (MBP)

Staining for myelin was lacking in immature brain (postnatal day 7 or 8) with positive staining being observed by 2 w of age (1 w post hypoxia–ischemia). In HI injured brain, there was less MBP staining in the ipsilateral cortex and ipsilateral cerebral peduncle at 1 and 4 w post hypoxia–ischemia (e.g. Fig. 3G). Considering the immaturity of the brain at the time of injury, the lower myelin staining (higher gray values) at 1 and 4 w post-insult ipsilaterally reflects less extensive myelin development on fewer axons within the ipsilateral than contralateral cerebral peduncle. Quantitatively, this resulted in ipsilateral–contralateral differences ($P < 0.01$) in gray levels of myelin basic protein staining of 2.15 ± 0.31% and 2.57 ± 1.2% at 1 and 4 w post HI, respectively.

3.2.3. Neuronal death detection with fluorojade staining

There were relatively few cells staining positively for fluorojade in sham control brain (e.g. Fig. 4A) or in brain regions contralateral to the cerebral hypoxia–ischemia. In the parietal cortex ipsilaterally, particularly in directly ischemic regions, there were numerous positively stained fluorojade neurons at all times after hypoxia–ischemia investigated (e.g. Fig. 4B–D). This was reflected in the quantitative assessment

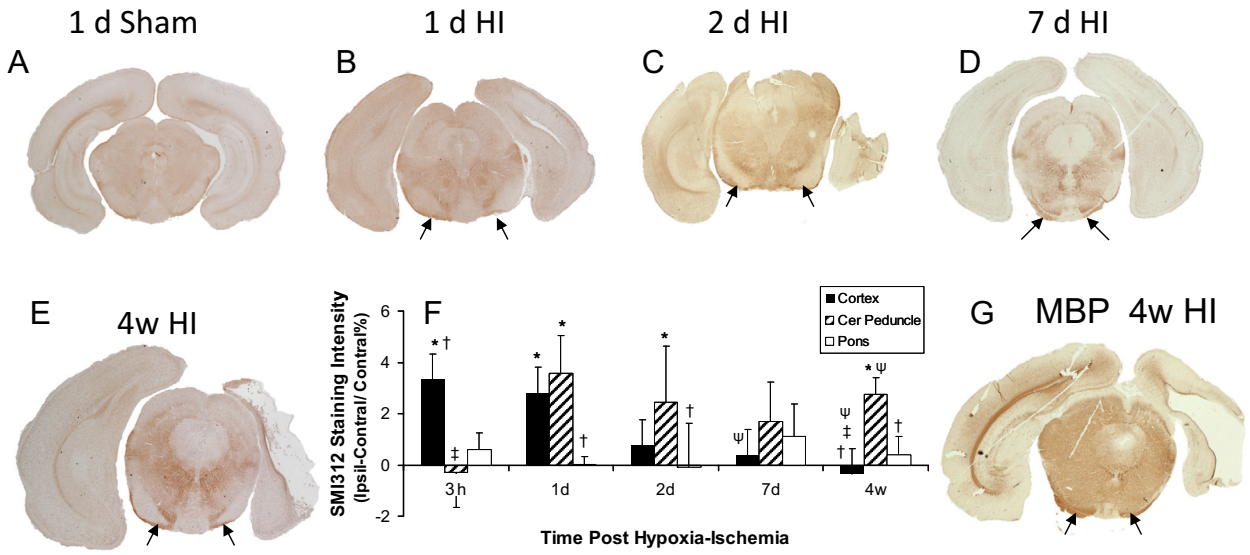

Fig. 3. Representative sections stained for axonal neurofilament using SMI312 immunohistochemistry (A–E). Quantitative differences of gray levels in the ipsilateral (Ipsil) and contralateral (Contral) hemisphere were presented as a % of Contral (panel F), there were significant reductions in gray level ipsilateral to the hypoxia–ischemia (HI), in the parietal cortex at 3 h and 1 d. Cerebral peduncle (arrows) showed decreased gray levels at acute and chronic time points (1 d to 4 w). Also shown is a representative section demonstrating diminished myelin basic protein (MBP) staining within the cerebral peduncle at 4 w following HI (G). Data are presented as mean ± SD. $^{*}P < 0.05$; ipsilateral different from contralateral; $^{\dagger}P < 0.05$, cortex or pons different from cerebral peduncle within the time point; $^{\ddagger}P < 0.05$, different from corresponding region at 1 d; $^{\Psi}P < 0.05$ different from corresponding region at 3 h (Two Way repeated ANOVA, Holm–Sidak multiple comparisons).

which also demonstrated an increase in the numbers of positive cells over time (Fig. 4G). In contrast to the cortex, the cerebral peduncle region had few positively stained cells, with the exception of 2 d following hypoxia–ischemia. At this time point appreciable numbers of fluorojade cells were observed ipsilaterally in 5/7 animals (median of 77 per field of view) in a region anatomically consistent as the pedunculopontine nucleus (e.g. Fig. 4E–F). This region has inputs/outputs to ischemic infarct regions. In the pons, there were few fluorojade stained cells and considered over all times, the mean numbers of fluorojade stained cells were not elevated significantly in either cerebral peduncle or pons (Fig. 4G).

1.2.4. Increased reactive astrocyte detection with staining for glial fibrillary acidic protein (GFAP)

Brains of sham animals (e.g. Fig. 5A) or brain contralateral to the hypoxia–ischemia had mild staining of astrocytes for GFAP (e.g. Fig. 5B). In the parietal cortex there was increased GFAP staining visible in directly ischemically injured regions at acute times (e.g. at 2 d and 4 w in Fig. 5C and D, respectively) and in pericyst regions at chronic times post-hypoxia–ischemia. Quantitatively, gray levels in the parietal cortex showed a significant percentage difference in ipsilateral versus contralateral values at 1 d to 4 w times post hypoxia–ischemia (Fig. 5G). In contrast, in the cerebral peduncle, there was some increased GFAP

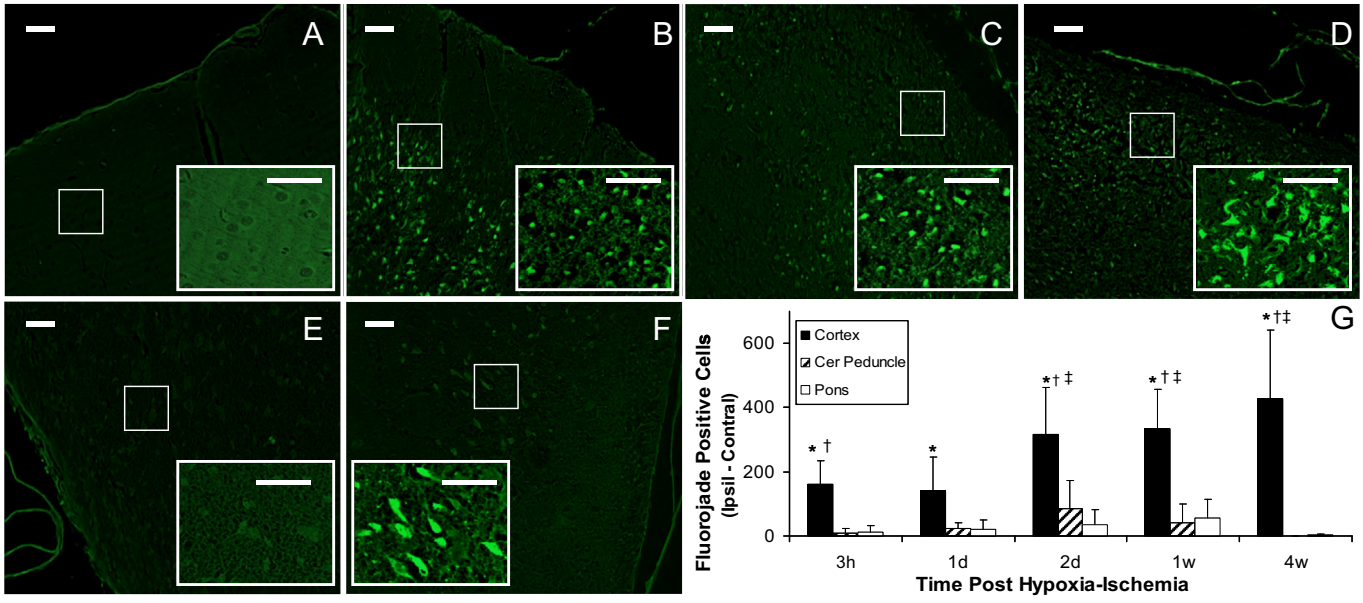

Fig. 4. Neuronal cell death detected with fluorojade staining at various times after transient unilateral cerebral hypoxia–ischemia. Shown are representative sections from parietal cortex of a control rat with sham surgery (A) and from cortex at 2 h, 2 d and 4 w after hypoxia–ischemia (B—D, respectively). The fluorojade positive cells are readily seen within the higher magnification insets for each micrograph (scale bars = 50 μm). Positive stained cells in the cerebral peduncle region at 2 d post insult are observed ipsilateral (F) but not contralaterally (E). The quantitative differences in numbers of stained cells per field of view ipsilaterally compared to that contralaterally after hypoxia–ischemia was significant only for parietal cortex (G). Data are presented as mean ± SD. $^{*}P < 0.05$; ipsilateral different from contralateral; $^{\dagger}P < 0.05$, cortex or pons different from cerebral peduncle within the time point; $^{\ddagger}P < 0.05$, different from corresponding region at 3 h and 1 d (Two Way repeated ANOVA, Holm–Sidak multiple comparisons).

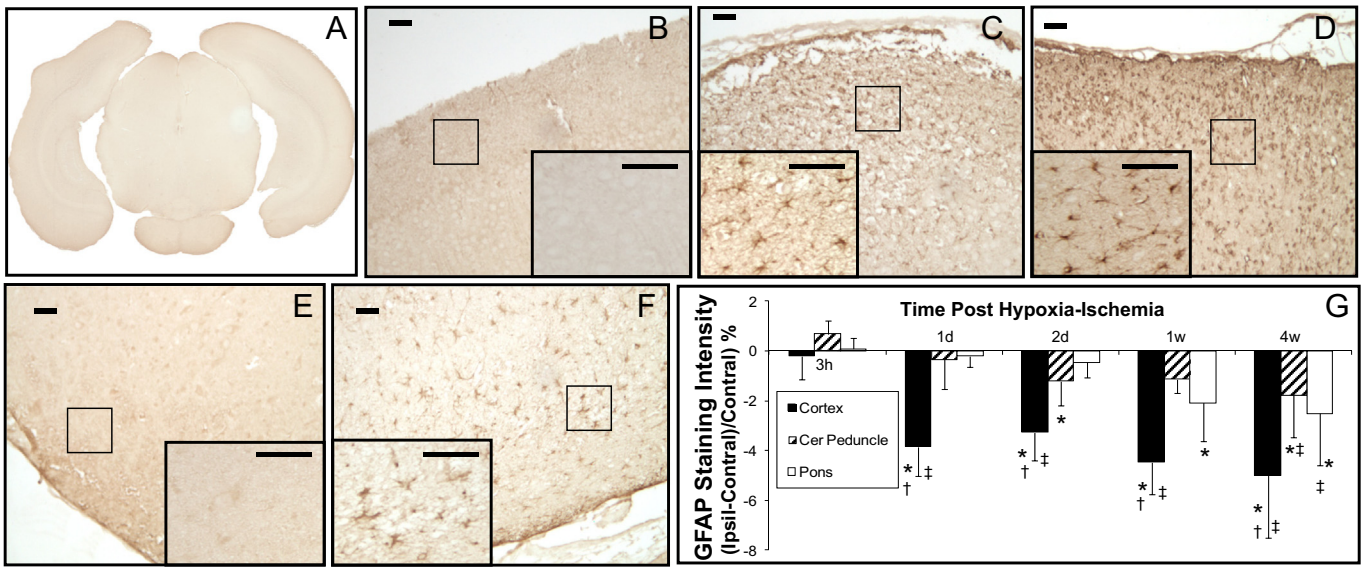

Fig. 5. Sections stained for astrocyte reactivity using GFAP immunohistochemistry. Examples of mild astrocytic staining shown in a digitized scan of a brain section from a sham P9 rat (A) and in parietal cortex (B) contralateral to the hypoxia–ischemia at 2 d post HI. Following hypoxia–ischemia in the parietal cortex, there was increased astrocyte reactivity ipsilaterally (e.g. at 2 d and 4 w post-insult in C and D, respectively). The GFAP positive cells are readily seen within the higher magnification insets (scale bars = 50 μm). This was reflected in quantitative measures of gray level changes in digitized sections with increased ipsilateral–contralateral differences in staining at all time points greater than 3 h. Also in cerebral peduncle, GFAP staining was increased ipsilaterally as shown in contralateral (E) and ipsilateral (F) sections of cerebral peduncle at 2 d post hypoxia–ischemia. Data are presented as mean ± SD. $^{*}P < 0.05$; ipsilateral different from contralateral; $^{\dagger}P < 0.05$, cortex or pons different from cerebral peduncle within the time point; $^{\ddagger}P < 0.05$, different from corresponding region at 3 h (Two Way repeated ANOVA, Holm–Sidak multiple comparisons).

staining of reactive astrocytes ipsilateral to the hypoxia–ischemia compared to that contralaterally but this was not evident until 2 d post insult (e.g. Fig. 5E, F) and was reflected in quantitative staining differences between 1 and 2 d (Fig. 5G). The pons was generally unaffected by hypoxia–ischemia at acute times but had some positive staining of reactive astrocytes at chronic (1 and 4 w) times post insult.

3.2.5. Increased microglia/macrophage staining using ED1/CD68 immunohistochemistry

In sham animals or in brain regions contralateral to the unilateral transient hypoxia–ischemia, there was no staining of activated microglia/macrophages (e.g. Fig. 6A, D). Within ischemically damaged parietal cortex, there were increased numbers of ED1/CD68 stained microglia/

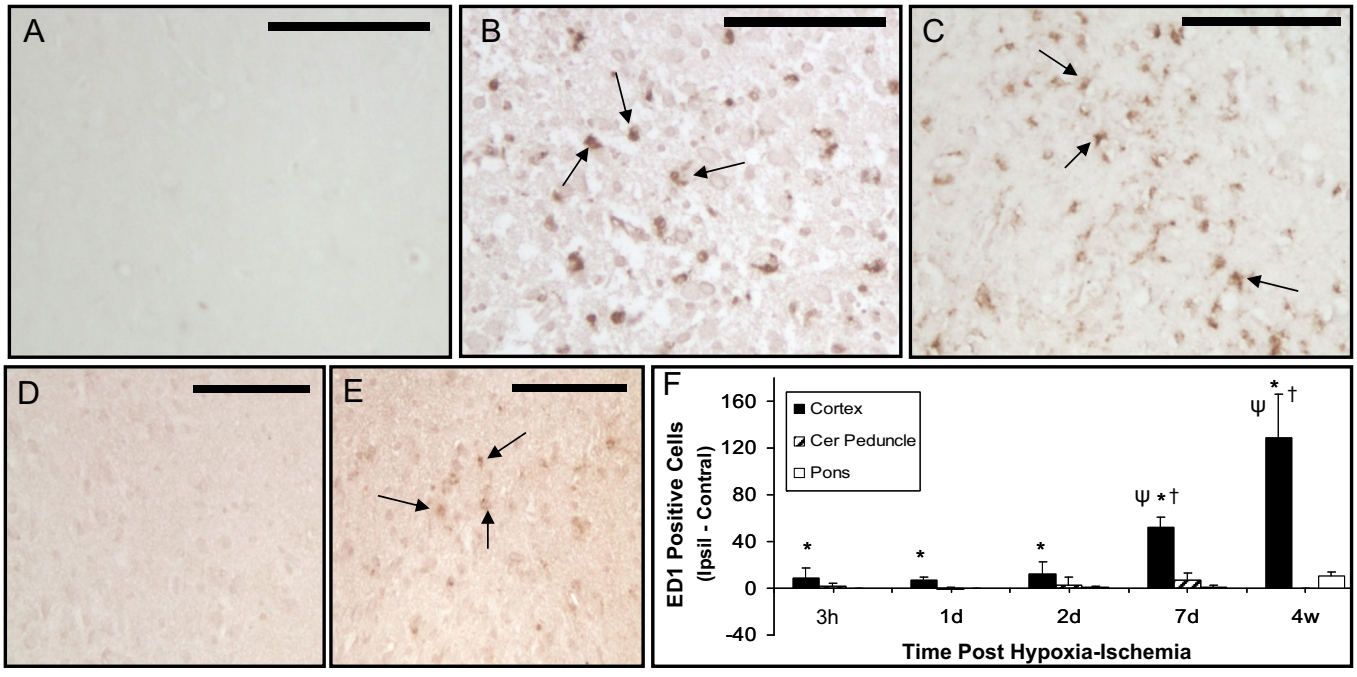

Fig. 6. ED1/CD68 positively stained activated microglia/macrophages following unilateral cerebral hypoxia–ischemia in neonatal rats. Minimal positive staining was observed in parietal cortex or cerebral peduncle contralateral to the hypoxia–ischemia (A, D, respectively). Increased numbers of positive stained cells (arrows) were observed in ipsilateral ischemic cortex (e.g. at 2 d (B) and 4 W (C) post hypoxia–ischemia). Increased positive staining in cerebral peduncle was observed in a few animals at 2 d and 1 w post hypoxia–ischemia with a representative example of left and right cerebral peduncle shown in D and E, respectively. Quantitative mean differences in ipsilateral (Ipsil)–contralateral (Contral) of the numbers of ED1/CD68 positively stained cells are shown in F. Data presented as mean ± S.D. $^{*}P < 0.05$; ipsilateral different from contralateral; $^{\dagger}P < 0.05$, cortex or pons different from cerebral peduncle within the time point; $^{\Psi}P < 0.05$, different from cortical values at earlier times (Two Way repeated ANOVA, Holm–Sidak multiple comparisons). Scale bar = 100 μm.

macrophages (e.g. Fig. 6B, C) which corresponded to increased numbers of positive cells ipsilaterally compared to contralaterally at all time points investigated. Quantitatively these changes were maximal at 4 w (Fig. 6F). In the cerebral peduncle, positive staining was not observed at acute (3 h–1 d) or chronic (4 w) time points but positive staining was observed in a few animals at subacute times (e.g. 4/12 animals at 2 d–1 w) post hypoxia–ischemia (Fig. 6E). However, over all times the mean numbers of positively stained ED1 cells was not elevated significantly in either cerebral peduncle or pons (Fig. 6F).

3.3. Correspondence between MRI and histological measures

An assessment of the potential contributions of various ischemic cellular responses to the DTI alterations was also performed by plotting schematically the mean changes in the DTI parameters within cerebral cortex or cerebral peduncle regions (Fig. 7A, B, respectively) or mean alterations in cellular markers within these regions (Fig. 7C, D). These plots highlight the different progression of the histological and MR variations over time in ischemic cortex and cerebral peduncle.

Within the parietal cortex, the DTI changes consisted of decreases in radial diffusivity, ADC, and parallel diffusivity that were maximal already at very early times corresponding to a maximal ipsilateral reduction in neurofilament staining and evidence of substantial cell injury detected with the fluorojade staining (Fig. 7A, C). Changes in T_2 and FA peaked around 1–2 d post insult corresponding to the onset of astrogliosis. However, there was a continued inflammatory response with astrogliosis and an increased microglial activation at more chronic times (1 and 4 w) that did not correspond well with the chronic normalization of the MR imaging. At chronic times the normalization of neurofilament staining differences appeared to correspond best to the chronic MR profile, although the signs of injury progression including astrogliosis, microgliosis and cell death do match the chronic increases in ADC and parallel diffusivity.

In the cerebral peduncle (Fig. 7B, D), all DTI parameters were maximally reduced ipsilaterally at 1 d post-insult and changes in T_2 were also maximally increased at this time. Subsequently there was in general normalization of MR changes with the exceptions of FA, some persistent reduction in parallel diffusivity along with an increased radial diffusivity ipsilaterally at chronic times. The acute and chronic changes in FA correspond well to the reduced staining for pan-axonal neurofilaments that became evident at 1 d. The appearance of increased astrogliosis and decreased myelination at chronic times parallel some of the persistent ADC and chronic radial diffusivity changes.

These complex data sets were also compared statistically. Significant correlations between changes in DTI and histological parameters were obtained for the cerebral cortex but not the cerebral peduncle, when considering all time points. Reductions in ADC and parallel diffusivity within the cerebral cortex were correlated to increased cell death, astrocyte reactivity (GFAP) or microglial/macrophage activation (ED1/CD68) ($R = 0.57$ ($p < 0.05$), $R = 0.63$ ($p < 0.02$), $R = .65$ ($p < 0.01$), respectively). Similarly there was a correlation between T_2 lesion size and decreases in ADC or parallel diffusivity within the cortex but not cerebral peduncle. Larger sample sizes in future studies could allow for multivariate comparisons between regions with sufficient power. Low (n.s.)

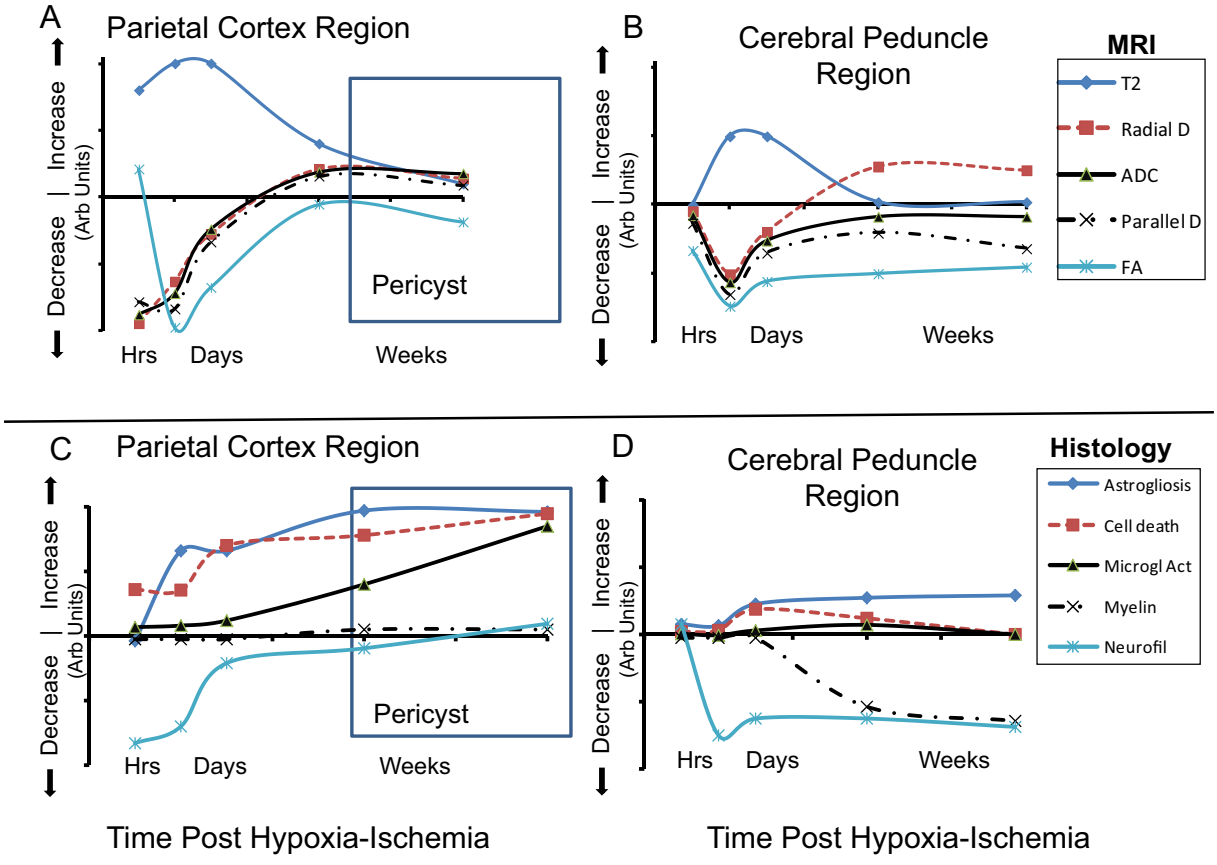

Fig 7. Schematic comparison of changes in MR imaging (A, B) and histology (C, D) in regions of ipsilateral ischemic cortex (A, C) and cerebral peduncle (B, D). Plots of relative alterations in arbitrary (Arb) units for each measure are presented over time post hypoxia–ischemia starting at 3 h post-insult. MR and histological values were initially unaffected, increased or decreased and subsequently changed with various profiles over time. Average T_2 changes from Lama et al. (2011) and Tuor et al. (2013). Abbreviations: D — diffusivity. FA — fractional anisotropy, Microgl Act — microglial/macrophage activation.

correlation of comparisons within time groups also likely reflects the modest ranges of insult severities considering that animals with either minimal or extensive injury were excluded.

4. Discussion

Despite intensive investigation of DTI's ability to detect brain injury, the interpretation of alterations in DTI measures is usually speculative because of a lack of direct documentation of the corresponding histological changes. In the present study we report detailed differences in the progression and magnitude of DTI and histological changes that provide a reference for identifying the potential contribution of various cellular responses to FA and axial, radial and mean diffusivity. The results are first to characterize the correspondence of the progression of cellular and DTI changes within the cerebral peduncle of the descending corticospinal tract following hypoxic–ischemic damage to the cortex. Novel is the demonstration of the differing progression of DTI alterations in a directly damaged ischemic region such as parietal cortex versus that in associated subcortical tracts. DTI changes were less severe or delayed in the cerebral peduncle of the corticospinal tract and this in general corresponded to less severe and delayed cellular responses consistent with early Wallerian degeneration. As discussed in more detail, the tissue alterations following ischemia and axonal degeneration had a complex relationship with changes in FA, parallel diffusivity and radial diffusivity.

Regarding our assessment of progressive changes in the DTI parameters, it is important to realize that superimposed on the effects of HI injury are well recognized developmental changes in the DTI parameters that occur during development and aging (Dubois et al., 2013). We controlled for this by making ipsilateral–contralateral comparisons which were then considered to reflect changes due to injury. Indeed, the contralateral hemisphere was similar to those in sham animals but developmental changes may have been differentially affected in the left and right hemispheres by the ischemic insult. Thus, the interpretation of left–right differences needs to include an awareness that these can be accounted for by an injury modulation of cellular maturation processes in white matter, which we assessed in our histological sections.

Another potential methodological limitation is varying contributions from partial volume effects over time. The region of cerebral peduncle measured was approx 0.3–0.4 mm^2 consisting of approx 10 pixels of sizes 0.024 mm^2 in the neonatal scans and 0.038 mm^2 in 5 wk old animals. Partial volume effects could be greater in neonatal brain than older brain. However, because we compared left and right differences in values, we expect that there were similar ipsilateral and contralateral partial volume effects in the cerebral peduncle at each time point. Partial volume effects in neonatal brains might diminish left–right differences but this did not appear to be an issue considering that many of our measures had the maximal changes in our neonates (e.g. 1 d post insult).

There have been numerous studies regarding the evolution of ADC or mean diffusivity following transient cerebral ischemia in regions of stroke. ADC alterations reported previously are comparable to those observed presently (e.g. Lama et al., 2011; Liu et al., 2007). Notably, there were striking similarities between the ADC and parallel diffusivity changes suggesting that both reflect similar cellular responses to injury. Very early ADC and parallel diffusivity changes in *ischemic cortex* are likely due to a greater restriction of water diffusion as a result of cytotoxic edema, reduced extracellular space and increased tortuosity which in the present study was also accompanied by decreased neurofilament staining and increased neuronal cell death. As vasogenic edema and damage to cellular membranes proceeded, which histologically corresponded to a continuing cell death and microglial/macrophage activation and astrogliosis, the reductions in ADC and parallel diffusivity normalized and this process occurred over several days. By 1–4 w, phagocytosis produced cysts in the infarct region and such cystic regions had an extremely large ADC in all directions whereas peri-infarct regions generally had normalized ADC and normalized parallel diffusivity despite the presence of inflammatory cells.

In contrast, in the *cerebral peduncle* with indirect ischemic injury, by the first 3 h there were modest but significant ADC and parallel diffusivity reductions. The hyperacute changes in ADC and parallel diffusivity correspond to our previous observation of a reduction in SMI31, demonstrating a decrease in phosphorylated heavy neurofilament subunits already hours after insult. Subsequently, the ADC and parallel diffusivity reductions increased in magnitude and were maximal in the first few days. This corresponded well with the diminished staining observed for the pan-axonal (heavy, medium and light) neurofilament marker SMI312 used presently. Loss of phosphorylation of neurofilaments promotes their disassembly and this corresponded to a decreased radial diffusivity as well as a decreased parallel and mean diffusivity of water. At chronic time points post-insult (1–4 w), parallel diffusivity remained sensitive to degenerative changes whereas ADC in the cerebral peduncle normalized. A similar greater sensitivity for parallel diffusivity than ADC in detecting Wallerian degenerative changes in the corticospinal tract has been reported after an excision lesion of the feline cortex (Qin et al., 2012). Microglial/macrophage cell activation likely did not contribute greatly to the parallel diffusivity alterations observed, considering the rather modest positive ED1/CD68 staining observed in the cerebral peduncle. The occurrence of astrogliosis coincided with normalization of ADC potentially contributing to some extent to these changes. However, as discussed below, there were also ipsilateral increases in radial diffusivity that likely contributed to the ADC normalization.

Reductions in radial diffusivity have been proposed to reflect well increases in myelin whereas elevations in radial diffusivity have been found to be associated with a loss of myelin (Song et al., 2002, 2004; Sun et al., 2008). The current study provides some support for this if one examines only chronic recovery times — i.e. times when the axons in the contralateral cerebral peduncle have become well myelinated. At 1 w and beyond, myelin within the cerebral peduncle ipsilaterally was reduced reflecting less ontogenic myelination of fewer axons following their degeneration and atrophy. This coincided with relative increases in radial diffusivity ipsilaterally and is consistent with increases in radial diffusivity reported in the corticospinal or pyramidal tracts at relatively chronic times (e.g. 1 w to 3 y) following an ischemic insult in children or adults (Roze et al., 2012; Yu et al., 2009; Zanier et al., 2013). At acute times post-insult we observed ipsilateral reductions in radial diffusivity within the cerebral peduncle indicating that in the absence of effects on myelination, early axonal injury such as that detected by decreases in phosphorylated neurofilaments were also associated with reduced radial diffusivity.

It is noteworthy that the neurophysiological correlates of alterations in parallel and radial diffusivity are potentially more complex in humans than rodents. A diffusion tensor analysis has an implicit assumption that the white matter fibers are cylindrical and when fibers have complicated microstructures or crossing fibers as occurs in human developing brain (Dubois et al., 2013; Jeurissen et al., 2013) then in particular the directions of orientation for tractography require careful interpretation. Despite crossing fibers potentially complicating the interpretation of parallel diffusivity changes, transverse or radial diffusivity appears to consistently decrease with all maturational processes within white matter, including myelination (Dubois et al., 2013). Furthermore, emerging imaging methods exploring diffusion parameters beyond the tensor model may provide more in depth assessments to facilitate translation from animals to humans (Dubois et al., 2013; Farquharson et al., 2013).

The FA measures provided a sensitive measure of direct ischemic injury. In the cortex at hyperacute times, there was an increase in FA, as has been observed previously in rats and non-human primates, however, usually soon after permanent rather than transient occlusion (Kim et al., 2013; Liu et al., 2007; Yang et al., 1999). This suggests that the very early cortical ischemic changes were relatively severe and similar to those with permanent ischemia. Cellular changes likely involve previously established hyperacute cytotoxic cell swelling and reductions in

extracellular space leading to cell death considering our histological evidence for hyperacute neuronal cell death in the cortex. By the first day post-insult, the FA increase became a decrease that persisted at subacute and chronic time points, confirming previous reports of a reduced FA commonly observed in damaged brain post-stroke (e.g. Kim et al., 2013; Liu et al., 2007; Yang et al., 1999). This decrease in FA, reflecting diminished preferential diffusivity, is likely associated with a loss of membrane integrity and intracellular structure due to necrosis as supported histologically by continuing cell death and loss of neurofilament staining. The increase in astrogliosis between 3 and 1 d appears rather isotropic considering that there is a decline in FA between these times.

The FA also provided a rather robust measure of degenerative changes in the cerebral peduncle. In contrast to ischemic cortex, FA in cerebral peduncle was decreased at all time points. Indeed, FA appeared to be the most sensitive DTI parameter for detecting axonal degenerative changes in the cerebral peduncle independent of time post-insult and this corresponded well to the persistent decreases in axonal neurofilament staining. Similar reductions in FA have been reported at various select times in the corticospinal tract following neonatal stroke (Ludeman et al., 2008; Puig et al., 2013; Tusor et al., 2012). It is currently clear that at chronic times, FA is superior to ADC or other standard imaging methods such as T2 imaging because lesions detected with these other sequences tended to pseudo-normalize at times post-insult (Lama et al., 2011; Tuor et al., 2013).

To conclude, the results demonstrate that in general, diffusivity changes and histological responses within directly damaged ischemic brain precede and are often larger in magnitude than corresponding alterations in a region of secondary axonal degeneration, such as the cerebral peduncle. With the progression of damage over one or more weeks, DTI components such as FA and radial diffusivity are better than mean ADC for detecting ischemia associated axonal injury indicative of Wallerian degeneration. Also, differences in radial diffusivity in brain injured perinatally are likely related to a lack of ontogenic myelination on the injured side. Thus, the specific progression of DTI alterations following an ischemic insult not only depends on the maturity of the subject but also appears dependent on other factors such as the type of insult (e.g. spinal cord injury or brain resection) (Brennan et al., 2013; Liu et al., 2013; Qin et al., 2012). The inflammatory response investigated (microglial or astroglial activation) appears to have modest contributions to the evolution of axonal changes in diffusion tensor parameters. Thus, this systematic study is informative regarding the optimal DTI MR imaging parameters to probe axonal injury following hypoxic/ischemic brain damage in developing brain in addition to aiding our interpretation of DTI parameters for detecting various stages of Wallerian degeneration.

Acknowledgements

The authors thank J. Hodge for informative exchanges regarding her methods of DTI analysis of the corticospinal tract. This study was supported by funding from the Heart and Stroke Foundation of Alberta, NWT and Nunavut and Canadian Institutes of Health Research (Grant MOP 111037). MS and MM were supported by studentships from Alberta Innovates Health Solutions and Markin USRP, respectively.

References

Brennan, F.H., Cowin, G.J., Kurniawan, N.D., Ruitenberg, M.J., 2013. Longitudinal assessment of white matter pathology in the injured mouse spinal cord through ultra-high field (16.4 T) in vivo diffusion tensor imaging. Neuroimage 82, 574–585. http://dx.doi.org/10.1016/j.neuroimage.2013.06.01923770410.

De Vries, L.S., Van der Grond, J., Van Haastert, I.C., Groenendaal, F., 2005. Prediction of outcome in new-born infants with arterial ischaemic stroke using diffusion-weighted magnetic resonance imaging. Neuropediatrics 36, 12–20. http://dx.doi.org/10.1055/s-2005-83754415776318.

Domi, T., deVeber, G., Shroff, M., Kouzmitcheva, E., MacGregor, D.L., Kirton, A., 2009. Corticospinal tract pre-Wallerian degeneration: a novel outcome predictor for pediatric stroke on acute MRI. Stroke; a Journal of Cerebral Circulation 40, 780–787. http://dx.doi.org/10.1161/STROKEAHA.108.52995819131656.

Dubois, J., Dehaene-Lambertz, G., Kulikova, S., Poupon, C., Hüppi, P.S., Hertz-Pannier, L., 2013. The early development of brain white matter: a review of imaging studies in fetuses, newborns and infants. Neuroscience http://dx.doi.org/10.1016/j.neuroscience.2013.12.04424378955.

Farquharson, S., Tournier, J.D., Calamante, F., Fabinyi, G., Schneider-Kolsky, M., Jackson, G.D., Connelly, A., 2013. White matter fiber tractography: why we need to move beyond DTI. Journal of Neurosurgery 118, 1367–1377. http://dx.doi.org/10.3171/2013.2.JNS12129423540269.

Hodge, J., 2013. Corticospinal Tract Diffusion Tensor Imaging and Motor Function in Children following Perinatal Stroke, http://theses.ucalgary.ca/handle/11023/397.

Jeurissen, B., Leemans, A., Tournier, J.D., Jones, D.K., Sijbers, J., 2013. Investigating the prevalence of complex fiber configurations in white matter tissue with diffusion magnetic resonance imaging. Human Brain Mapping 34, 2747–2766. http://dx.doi.org/10.1002/hbm.2209922611035.

Jiang, H., Van Zijl, P.C., Kim, J., Pearlson, G.D., Mori, S., 2006. DtiStudio: resource program for diffusion tensor computation and fiber bundle tracking. Computer Methods and Programs in Biomedicine 81, 106–116. http://dx.doi.org/10.1016/j.cmpb.2005.08.00416413083.

Kim, J.H., Na, D.G., Chang, K.H., Song, I.C., Choi, S.H., Son, K.R., Kim, K.W., Sohn, C.H., 2013. Serial MR analysis of early permanent and transient ischemia in rats: Diffusion tensor imaging and high b value diffusion weighted imaging. Korean Journal of Radiology: Official Journal of the Korean Radiological Society 14, 307–315. http://dx.doi.org/10.3348/kjr.2013.14.2.30723482695.

Kirton, A., Shroff, M., Visvanathan, T., deVeber, G., 2007. Quantified corticospinal tract diffusion restriction predicts neonatal stroke outcome. Stroke; a Journal of Cerebral Circulation 38, 974–980. http://dx.doi.org/10.1161/01.STR.0000258101.67119.7217272775.

Lama, S., Qiao, M., Kirton, A., Sun, S., Cheng, E., Foniok, T., Tuor, U.I., 2011. Imaging corticospinal degeneration in neonatal rats with unilateral cerebral infarction. Experimental Neurology 228, 192–199. http://dx.doi.org/10.1016/j.expneurol.2011.01.00221223967.

Latchaw, R.E., Alberts, M.J., Lev, M.H., Connors, J.J., Harbaugh, R.E., Higashida, R.T., Hobson, R., Kidwell, C.S., Koroshetz, W.J., Mathews, V., Villablanca, P., Warach, S., Walters, B., 2009. Recommendations for imaging of acute ischemic stroke: a scientific statement from the American Heart Association. Stroke; a Journal of Cerebral Circulation 40, 3646–3678. http://dx.doi.org/10.1161/STROKEAHA.108.19261619797189.

Liu, M., Gross, D.W., Wheatley, B.M., Concha, L., Beaulieu, C., 2013. The acute phase of Wallerian degeneration: longitudinal diffusion tensor imaging of the fornix following temporal lobe surgery. Neuroimage 74, 128–139. http://dx.doi.org/10.1016/j.neuroimage.2013.01.06923396161.

Liu, Y., D'Arceuil, H.E., Westmoreland, S., He, J., Duggan, M., Gonzalez, R.G., Pryor, J., de Crespigny, A.J., 2007. Serial diffusion tensor MRI after transient and permanent cerebral ischemia in nonhuman primates. Stroke; a Journal of Cerebral Circulation 38, 138–145. http://dx.doi.org/10.1161/01.STR.0000252127.07428.9c17122422.

Ludeman, N.A., Berman, J.I., Wu, Y.W., Jeremy, R.J., Kornak, J., Bartha, A.I., Barkovich, A.J., Ferriero, D.M., Henry, R.G., Glenn, O.A., 2008. Diffusion tensor imaging of the pyramidal tracts in infants with motor dysfunction. Neurology 71, 1676–1682. http://dx.doi.org/10.1212/01.wnl.0000304084.59964.e218448871.

Nucifora, P.G., Verma, R., Lee, S.K., Melhem, E.R., 2007. Diffusion-tensor MR imaging and tractography: exploring brain microstructure and connectivity. Radiology 245, 367–384. http://dx.doi.org/10.1148/radiol.2452060445179403000.

Paxinos, G., Watson, C., 1998. The Rat Brain in Sterotaxic CoordinatesFourth edition. Academic Press, New York.

Puig, J., Blasco, G., Daunis-I-Estadella, J., Thomalla, G., Castellanos, M., Figueras, J., Remollo, S., van Eendenburg, G., Sánchez-González, J., Serena, J., Pedraza, S., 2013. Decreased corticospinal tract fractional anisotropy predicts long-term motor outcome after stroke. Stroke; a Journal of Cerebral Circulation 44, 2016–2018. http://dx.doi.org/10.1161/STROKEAHA.111.00038223652266.

Qiao, M., Meng, S., Foniok, T., Tuor, U.I., 2009. Mild cerebral hypoxia–ischemia produces a sub-acute transient inflammatory response that is less selective and prolonged after a substantial insult. International Journal of Developmental Neuroscience: The Official Journal of the International Society for Developmental Neuroscience 27, 691–700. http://dx.doi.org/10.1016/j.ijdevneu.2009.07.00419631731.

Qin, W., Zhang, M., Piao, Y., Guo, D., Zhu, Z., Tian, X., Li, K., Yu, C., 2012. Wallerian degeneration in central nervous system: dynamic associations between diffusion indices and their underlying pathology. PloS One 7, e41441. http://dx.doi.org/10.1371/journal.pone.0041441222829950.

Roze, E., Harris, P.A., Ball, G., Elorza, L.Z., Braga, R.M., Allsop, J.M., Merchant, N., Porter, E., Arichi, T., Edwards, A.D., Rutherford, M.A., Cowan, F.M., Counsell, S.J., 2012. Tractography of the corticospinal tracts in infants with focal perinatal injury: comparison with normal controls and to motor development. Neuroradiology 54, 507–516. http://dx.doi.org/10.1007/s00234-011-0969-522006424.

Schmued, L.C., Hopkins, K.J., 2000. Fluoro-jade B: a high affinity fluorescent marker for the localization of neuronal degeneration. Brain Research 874, 123–13010960596.

Song, S.K., Kim, J.H., Lin, S.J., Brendza, R.P., Holtzman, D.M., 2004. Diffusion tensor imaging detects age-dependent white matter changes in a transgenic mouse model with amyloid deposition. Neurobiology of Disease 15, 640–647. http://dx.doi.org/10.1016/j.nbd.2003.12.00315056472.

Song, S.K., Sun, S.W., Ramsbottom, M.J., Chang, C., Russell, J., Cross, A.H., 2002. Dysmyelination revealed through MRI as increased radial (but unchanged axial) diffusion of water. Neuroimage 17, 1429–143612414282.

Sun, S.W., Liang, H.F., Cross, A.H., Song, S.K., 2008. Evolving Wallerian degeneration after transient retinal ischemia in mice characterized by diffusion tensor imaging. NeuroImage 40, 1–10. http://dx.doi.org/10.1016/j.neuroimage.2007.11.04918187343.

Tuor, U.I., Qiao, M., Morgunov, M., Fullerton, E., Foniok, T., Kirton, A., 2013. Magnetization transfer and diffusion imaging of acute axonal damage in the cerebral peduncle following hypoxia–ischemia in neonatal rats. Pediatric Research 73, 325–331. http://dx.doi.org/10.1038/pr.2012.17823202723.

Tusor, N., Wusthoff, C., Smee, N., Merchant, N., Arichi, T., Allsop, J.M., Cowan, F.M., Azzopardi, D., Edwards, A.D., Counsell, S.J., 2012. Prediction of neurodevelopmental outcome after hypoxic–ischemic encephalopathy treated with hypothermia by diffusion tensor imaging analyzed using tract-based spatial statistics. Pediatric Research 72, 63–69. http://dx.doi.org/10.1038/pr.2012.4022447318.

van der Aa, N.E., Leemans, A., Northington, F.J., van Straaten, H.L., van Haastert, I.C., Groenendaal, F., Benders, M.J., De Vries, L.S., 2011. Does diffusion tensor imaging-based tractography at 3 months of age contribute to the prediction of motor outcome after perinatal arterial ischemic stroke? Stroke; a Journal of Cerebral Circulation 42, 3410–3414. http://dx.doi.org/10.1161/STROKEAHA.111.62485822020032.

Vannucci, R.C., Vannucci, S.J., 2005. Perinatal hypoxic–ischemic brain damage: evolution of an animal model. Developmental Neuroscience 27, 81–86. http://dx.doi.org/10.1159/000085978160468840.

Yang, Q., Tress, B.M., Barber, P.A., Desmond, P.M., Darby, D.G., Gerraty, R.P., Li, T., Davis, S.M., 1999. Serial study of apparent diffusion coefficient and anisotropy in patients with acute stroke. Stroke; a Journal of Cerebral Circulation 30, 2382–2390 10548675.

Yu, C., Zhu, C., Zhang, Y., Chen, H., Qin, W., Wang, M., Li, K., 2009. A longitudinal diffusion tensor imaging study on Wallerian degeneration of corticospinal tract after motor pathway stroke. NeuroImage 47, 451–458. http://dx.doi.org/10.1016/j.neuroimage.2009.04.06619409500.

Zanier, E.R., Pischiutta, F., Villa, P., Paladini, A., Montinaro, M., Micotti, E., Orrù, A., Cervo, L., De Simoni, M.G., 2013. Six-month ischemic mice show sensorimotor and cognitive deficits associated with brain atrophy and axonal disorganization. CNS Neuroscience & Therapeutics 19, 695–704. http://dx.doi.org/10.1111/cns.1212823742688.

Zhang, J., Aggarwal, M., Mori, S., 2012. Structural insights into the rodent CNS via diffusion tensor imaging. Trends in Neurosciences 35, 412–421. http://dx.doi.org/10.1016/j.tins.2012.04.01022651954.